Materials Transactions, Vol. 56, No. 11 (2015) pp. 1834 to 1841

A Practical Investigation of the Production of Zr-Cu-Al-Ni Bulk Metallic Glasses by Arc Melting and Suction Casting

Joshua Igel[1,*], Donald W. Kirk[2], Chandra Veer Singh[1] and Steven J. Thorpe[1]

[1]*Department of Materials Science and Engineering, University of Toronto, 184 College St., Rm. 140, Toronto, Ontario M5S 3E4, Canada*
[2]*Department of Chemical Engineering & Applied Chemistry, University of Toronto, 200 College St., Toronto, Ontario M5S 3E5, Canada*

The successful fabrication of bulk metallic glasses (BMG) through suction casting based on the existing literature is a difficult task due to the sensitivity of glass-forming ability (GFA) to small changes in processing variables. We report processing challenges and process modifications required in the successful and consistent production of Zr-Cu-Al-Ni BMGs by arc melting and suction casting. Focus was placed on homogenization methods, elemental yields, and the effect of argon purge gas and Zr purity on GFA. A "cut and re-cast" homogenization method used to reduce oxidation produced good overall homogeneity but resulted in the entrainment of an oxide-rich surface layer into the bulk of the alloy. Homogenization by multiple melting iterations and prolonged melting times was ultimately found to be the most effective method. Zr loss was observed in the bulk of the samples post-production. This has been attributed to the formation of a Zr/ZrO_2 surface layer during melting. Using X-ray diffraction and isochronal DSC, both argon gas purity and Zr purity were shown to markedly affect GFA. GFA was optimized within a specific oxygen concentration range. The highest GFA was obtained when using high purity argon (Grade 6.0) and low Zr purity (99.5%). The optimization of GFA in Zr-based BMGs at a critical oxygen concentration has not been shown in previous work.
[doi:10.2320/matertrans.M2015235]

(Received June 8, 2015; Accepted July 28, 2015; Published October 2, 2015)

Keywords: *zirconium-based bulk metallic glasses, arc melting and suction casting, glass-forming ability*

1. Introduction

Bulk metallic glasses (BMGs) are a relatively new class of material with enhanced properties with respect to crystalline metals, such as higher strength, greater elastic strain limit and better corrosion resistance.[1–3] Unlike conventional metallic glasses, BMGs can be formed with thicknesses greater than 1 mm making them useful for structural applications.

There are a large number of BMG alloy systems which have been identified and investigated thus far. Zr-based BMGs are especially promising due to the combination of the low cost of raw materials and high glass-forming ability (GFA). The reported critical casting thicknesses of high GFA Be-free Zr-based alloys are typically between 20–25 mm with the largest being 30 mm for $Z_{55}Cu_{30}Al_{10}Ni_5$.[4] Currently, the GFA of Zr-based BMGs are only surpassed by Pd-based alloys which can achieve critical diameters as large as 80 mm.[5] However, Pd-based alloys are reserved for specialized purposes due to the high price of Pd.

In addition to composition selection, the production of fully amorphous BMGs involves the optimization of processing conditions. Laws *et al.* have shown that casting parameters such as casting temperature, casting velocity, mould temperature, mould surface roughness and mould geometry can significantly affect critical casting thickness by influencing interfacial heat transfer.[6] Understanding the interrelationship between compositional variations and processing condition is essential considering that small changes in the concentrations of the main alloying elements can strongly affect GFA.[7–11] Particularly in Zr-based BMGs, critical cooling rates have been found to be extremely sensitive to the concentration of oxygen impurities.[12–14] Although multiple studies have modified processing conditions to optimize GFA, it is usually difficult to find actual details of these parameters making reproduction of BMGs reported in these studies problematic.

This work specifically attempts to fill this gap in our understanding of the effects of processing variables in the production of Zr-based BMGs by arc melting and suction casting. In this study, we have specifically explored the following areas of the production of Zr-based BMGs by arc melting and suction casting: (a) homogenization methods, (b) elemental yields, and (c) the effect of argon purge gas and metallic Zr purity on GFA. Insights obtained from this analysis will contribute to the development of standard production methods with optimum conditions for obtaining high GFA BMGs.

2. Experimental Procedure

Ingots were prepared by arc melting pure Zr (99.5%), Cu (99.995%), Al (99.999%) and Ni (99.98%) in argon at atmospheric pressure. Rods with a diameter of 3 mm and length of 29.5 mm were produced by arc melting and suction casting of the ingots into a water-cooled copper mould. The melting chamber was purged by lowering the pressure to around 0.1 mbar using a roughing pump and subsequently re-filling the chamber with argon until atmospheric pressure was reached. This was repeated five times before melting and casting. Three different homogenization methods were explored, which have been named: 1) the standard method, 2) the conservative method, and 3) the cut and re-cast method. Detailed descriptions of the different homogenization methods are provided in the Results and Discussion section.

In order to analyze homogeneity across manufactured samples, cross-sections from the "top", "middle" and "bottom" of the cast rods (Rod A, B and C) were cut using

*Corresponding author, E-mail: josh.igel@mail.utoronto.ca

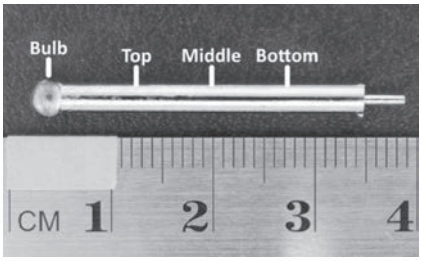

Fig. 1 Image of a suction cast rod showing the locations of the top, middle and bottom sections.

a diamond wheel cutter. The top section was taken at approximately a quarter of the length of the rod from the top, the middle section at half of the length and the bottom at three-quarters of the length. This is shown in Fig. 1. The sections were ground using SiC grinding paper and polished with diamond paste impregnated polishing cloths. In the final polishing step, 1 μm diamond paste was used. Scanning electron microscopy/energy dispersive spectroscopy (SEM/EDX) was utilized to determine bulk composition and observe microstructure. X-ray diffraction (XRD) was performed using a Rigaku MiniFlex 600 diffractometer with a Cu-Kα source to investigate the extent of crystallization.

The effect of argon and Zr purity on GFA was investigated by examining the microstructure, extent of crystallization, crystallization behaviour and thermal stability of rods produced using different grades of Ar purge gas and raw Zr (Rod A, E, F and G) purity. Crystallization behaviour and thermal stability were examined by isochronal differential scanning calorimetry (DSC) using a heating rate of 10 K/min. The impurity content of the different grades of Ar purge gas and raw Zr purity are shown in the Results and Discussion section.

3. Results and Discussion

3.1 Homogenization methods

$Zr_{55}Cu_{30}Al_{10}Ni_5$ was targeted for production since to date this composition has the largest reported critical casting diameter in the Zr-Cu-Al-Ni system.[4] Three rods (Rod A, B and C) of this nominal composition were produced each with a different homogenization method. Rod A was produced using the standard method. In this method, the ingot was melted, allowed to solidify, flipped and re-melted three subsequent times following the initial melting to consolidate the raw material before casting. In each pre-casting melting step, the arc was circled over the material for approximately 10 s. Four melting iterations were performed as is the standard practice reported in literature. After approximately 4 seconds of melting, the ingot appeared completely molten. Nonetheless, the time was prolonged to ensure enhanced mixing from the arc.

Table 1 shows the compositions of the top, middle and bottom sections of Rod A. Clearly, it can be seen that Rod A is homogeneous since the compositions of the different sections are observed to be practically identical. Interestingly, the compositions of the sections measured using EDX are noticeably different than the nominal (input) composition. Specifically, it is evident that Zr is depleted. The reason behind this was carefully investigated and will be discussed later in Section 3.2.

Table 1 Compositions of the top, middle and bottom cross-sections of Rod A, B and C in at% determined by EDX.

	Zr	Cu	Al	Ni
Rod A				
Top	52.7 ± 0.3	31.8 ± 0.5	10.3 ± 0.6	5.2 ± 0.3
Middle	52.6 ± 0.3	32.0 ± 0.5	10.2 ± 0.6	5.2 ± 0.3
Bottom	52.9 ± 0.3	31.3 ± 0.5	10.3 ± 0.6	5.5 ± 0.3
Rod B				
Top	47.4 ± 0.3	35.7 ± 0.5	11.4 ± 0.5	5.4 ± 0.3
Middle	43.6 ± 0.5	41.9 ± 0.7	8.3 ± 0.5	6.2 ± 0.5
Bottom	48.6 ± 0.3	34.9 ± 0.5	11.8 ± 0.5	4.7 ± 0.3
Rod C				
Top	51.7 ± 0.2	32.5 ± 0.2	10.5 ± 0.2	5.4 ± 0.3
Middle	52.6 ± 0.2	31.4 ± 0.2	10.7 ± 0.2	5.4 ± 0.3
Bottom	52.5 ± 0.3	31.6 ± 0.2	10.4 ± 0.2	5.5 ± 0.3

After casting, it was noticed that the colour of the bulb was different than the bulk of the rod as shown in Fig. 1. Colouration can be due to variation in the surface composition via segregation or due to the formation of a surface layer such as an oxide film. It was initially hypothesized that Cu was concentrated in the bulb due to poor mixing. However, the EDX results only showed a depletion of Zr, but not a Cu enrichment. Due to this, the segregation hypothesis was rejected.

It is reasonable to assume that an oxide-rich surface layer would concentrate in the bulb during casting due to buoyancy. However, the amount of oxygen contained in the argon purge gas and raw Zr as per the manufacturers' specifications was not sufficient to account for the observed depletion of Zr. It is quite possible that the oxide is firmly attached to a thick Zr substrate, and this may account for the observed Zr depletion. The oxide rich surface layer hypothesis may also explain the Cu colour of the bulb based on a study performed by Liu *et al.* which showed that oxidation in $Zr_{55}Cu_{30}Al_{10}Ni_5$ is accompanied by Cu precipitation on the outer surface of the oxide layer due to preferential oxidation of Zr and back-diffusion of Cu.[15] Note that Cu precipitation would only occur at the oxidized surface and should not affect the Cu concentration of the bulk of the rod.

An XRD spectrum of the middle section of Rod A in Fig. 2 shows that the rod is not fully amorphous due to the presence of diffraction peaks. The majority of these peaks have been identified to correspond to an icosahedral quasicrystalline phase (i-phase). This is supported by successful indexing of the icosahedral planes (based on a scheme described by Bancel and Heiney[16]). For some peaks, there are slight but noticeable differences between the observed and calculated peak positions. However, this is expected since rapidly cooled materials inevitably contain residual stresses which cause structural distortions.

The remaining peaks in Fig. 2 have been identified to correspond to monoclinic ZrO_2 (m-ZrO_2) and tetragonal ZrO_2

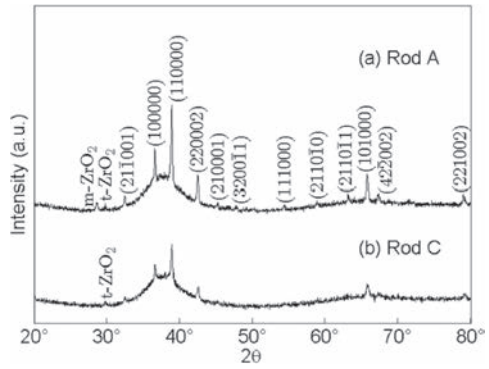

Fig. 2 XRD spectra obtained for the middle sections of (a) Rod A and (b) Rod C.

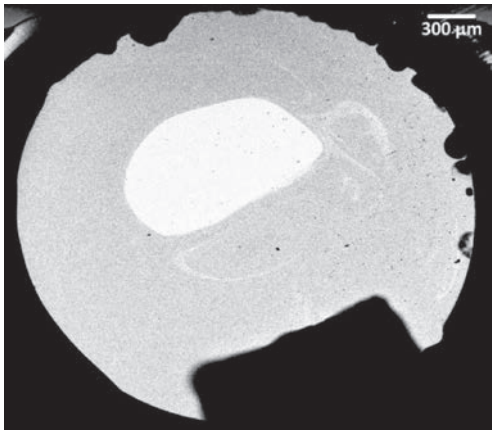

Fig. 3 BSE image of the bottom section of Rod C displaying local inhomogeneity. The dark section at the bottom right of the image is carbon tape used to electrically ground the sample.

(t-ZrO_2). Since the icosahedral phase has only been found to form in Zr-based BMGs when the dissolved oxygen content is above a critical value,[17] this suggests that the amount of dissolved oxygen in Rod A was above this threshold. The ZrO_2 observed in the spectrum may either have originated from the raw Zr or was formed by oxidation during melting.

Rod B was produced using the conservative method. In this method, the number of melting iterations and melting duration were decreased to reduce the extent of oxygen dissolution and oxidation in an attempt to improve GFA. The ingot was flipped and re-melted once after initially melting to consolidate the raw material. The ingot was then melted and suction cast. In each melting sequence, the arc was circled over the material for approximately 4 s.

As it can be seen in Table 1, the compositions of the top, middle and bottom sections of Rod B are significantly different. Also, the Zr concentrations of all sections from Rod B are lower than those in the homogenized Rod A, while the Cu concentrations are all higher. Furthermore, a concentration gradient can be seen in Rod B. Zr concentrations are higher in the top and bottom sections than in the middle section, while the copper concentrations are lower than in the middle section. These gradients imply that the melt must also have had a concentration gradient which would have been from the interior to the exterior of the melt pool. A vertical melt gradient would not produce the symmetrical gradients observed in Rod B.

Both Rod A and Rod B had copper coloured bulbs indicating that the decreased melting frequency and duration used for Rod B did not change the amount of surface oxidation. Nevertheless, the density difference and melting temperature difference between ZrO_2 and Zr is significant. The concentration gradients could still be oxide related but would appear to be from the initial Zr purity.

The cut and re-cast method (Rod C) was initially used in an attempt to reduce the surface oxidation by physical mixing. The cut and re-cast method was examined since it was postulated that it could be used to both reduce oxygen dissolution and oxidation, and ensure good mixing. In this method, the melting and casting procedure was identical to that of the conservative method except that following casting, the rods were cut into small pieces using a diamond wheel cutter and randomly mixed in the crucible prior to melting and casting. Cutting and re-casting was performed twice following the initial casting. The mixing of the cut pieces in the crucible provided the ability to mix without raising temperature and thus, could potentially reduce oxygen dissolution and oxidation without compromising homogeneity.

Interestingly, although the EDX analysis in Table 1 shows reasonable homogeneity, SEM imaging revealed that the cut and re-cast method promoted local inhomogeneity as shown in the BSE image of the bottom section of Rod C in Fig. 3 displaying a large bright region in the interior of the sample. EDX showed that this region contained Zr and O in a 3 : 1 ratio. Due to this, it is believed that this is a portion of the Zr/ZrO_2 surface layer, discussed earlier, which had become entrained into the bulk of the rod during re-casting. The ellipsoid shape of this region further supports this postulation since the surface of the bulb would have this shape if it were to be flattened. Despite the failure of the cut and re-cast technique, it is interesting to note that the compositions of the top, bottom and middle sections of Rod C shown in Table 1 are nearly identical to each other and those of Rod A. This suggests good overall homogeneity despite localized entrained regions of oxide. It should be noted that the bulk EDX spectrum for the bottom section of Rod C did not include the Zr/ZrO_2-rich region. The spectrum was taken in the surrounding matrix.

Like Rod A, Rod C contains i-phase and t-ZrO_2 as shown by the XRD spectrum in Fig. 2. The lower intensities of i-phase peaks in the Rod C spectrum suggest that less oxygen was dissolved during casting due to relationship between dissolved oxygen and i-phase formation described earlier. The similar intensities of the t-ZrO_2 peaks in the XRD spectra for Rod A and C suggests that they have similar t-ZrO_2 content. The extent of oxidation seems to be lower in Rod C due to the lack of the monoclinic ZrO_2 (m-ZrO_2) peak in the Rod C spectrum which are evident in the Rod A spectrum. This suggests that the use of the cut and re-cast method reduced oxygen availability by keeping ZrO_2 from dispersing in the melt. As such, the cut and re-cast method may be useful if entrainment of the surface oxide layer could be avoided. This can be achieved by discarding the bulb or removing the surface oxide by grinding before re-casting

after cutting. However, if the rod is not well-mixed before cutting, both of these would cause the final composition to vary from the target in a non-predictable manner. Due to the difficulty associated with avoiding local inhomogeneity, the cut and re-cast method is ultimately suboptimal. The decrease in the amount of i-phase and oxides associated with the cut and re-cast method was significant, but it does not seem probable that these phases could be completely eliminated by further modifications to the homogenization procedure. Controlling the extent of oxygen dissolution and oxidation by adjusting the purities of Ar purge gas and raw Zr is likely a more efficient alternative (discussed further in Section 3.3).

3.2 Elemental yields

As described earlier, the lower than nominal concentration of Zr in Rod A, B and C may suggest that a Zr/ZrO_2 layer separates from the bulk of the rod during casting. Interestingly, there is a negligible composition difference between Rod A and C as shown in Table 1. Based on the hypothesis that Zr depletion is caused by the formation of a Zr/ZrO_2 surface layer during melting and casting, the less oxidized Rod C should have a composition closer to the nominal. However, this may not necessarily be true if the majority of the oxide in the surface layer originates from the surface of the raw Zr powder so the extent of oxidation during casting would not have an appreciable effect on final composition. Based on the assumption that Zr depletion is due to the segregation of a Zr/ZrO_2 from the surface of the raw Zr during casting, the amount of Zr lost to the surface oxide layer should be directly proportional to the mass of raw Zr used. If the amount of Zr lost was related to oxidation during casting, it would be directly proportional to surface area. The Zr_{lost}/Zr_{used} constant can be obtained by calculating the amount of Zr lost using the following equation:

$$Zr_{lost}/Zr_{used} = (1 - [Zr]_{EDX}/[Zr]_{input})/(1 - [Zr]_{EDX})$$

where $[Zr]_{input}$ is the at. fraction of Zr in the input mixture as-weighed and $[Zr]_{EDX}$ is the at. fraction of Zr determined by EDX.

By utilizing the equation above, it was found that the Zr_{lost}/Zr_{used} value was relatively constant amongst Zr-Cu-Al-Ni rods with different compositions (approx. 90 mg/g) thus supporting the hypothesis. Table 2 shows the predicted and actual compositions for the middle section of Rod A using the Zr_{lost}/Zr_{used} constant. It can be seen that the predicted composition for the rod is nearly identical to the composition determined by EDX further supporting the hypothesis.

Based on above analysis, we corrected for the loss of Zr in the cast alloy by adding more Zr to the initial mix and a rod with input composition of $Zr_{55.8}Cu_{29.8}Al_{9.5}Ni_{4.9}$ (Rod D) was produced. This is closer to the composition of $Zr_{55}Cu_{30}Al_{10}Ni_5$ than the measured compositions of the rods previously discussed. An abundance of intermetallic crystals ($CuZr_2$ and $AlZr_3$) can be seen in the BSE image of Rod D shown in Fig. 4 alongside two amorphous phases ($Zr_{56}Cu_{30}Al_9Ni_5$ and $Zr_{53}Cu_{31}Al_{10}Ni_6$). In contrast, the BSE image of Rod A in Fig. 5(a) mainly shows a homogeneous amorphous matrix containing few small dendritic crystals. This shows that the GFA of Rod A is greater than that of Rod D. This is not surprising since the study discussing the 30 mm $Zr_{55}Cu_{30}Al_{10}Ni_5$ rod reported a nominal rather than measured composition.[4)]

Table 2 Compositions determined by EDX (actual) and predicted compositions of the middle section of Rod A. Values are in at%.

	Zr	Cu	Al	Ni
Actual	52.6 ± 0.3	32.0 ± 0.5	10.2 ± 0.6	5.2 ± 0.3
Predicted	52.6	31.6	10.5	5.3

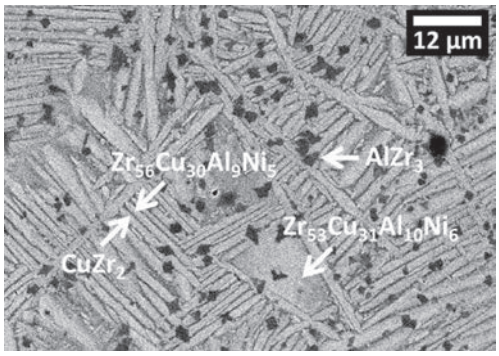

Fig. 4 BSE image of the heavily crystallized middle section of Rod D ($Zr_{55.8}Cu_{29.8}Al_{9.5}Ni_{4.9}$). Compositions of phases were determined using EDX.

Based on the assumption that the depletion of Zr is caused by the oxide from the surface of the raw Zr, the extent of depletion will depend only on the amount of oxide contained by the raw Zr. This will vary based on the method used to produce the raw Zr and its geometry. Without knowing these parameters, the actual composition of the reported alloy cannot be known with certainty. It is suggested that if a measured composition is reported, this should be sought as the final composition. In the remainder of this study, alloys were produced with a nominal composition of $Zr_{55}Cu_{30}Al_{10}Ni_5$.

3.3 Effect of argon and raw Zr purities on GFA

Table 3 shows the purity of Ar and Zr used to produce each rod (Rod A, E, F and G). Table 4 shows the concentrations of the main impurities in the Ar and Zr as provided by the suppliers. EDX showed that the compositions of the four rods in terms of the main metallic elements were practically identical. Therefore, the differences in GFA are solely based upon the concentrations of impurities.

No discernable evidence of crystallization can be observed in the BSE images of the middle sections of Rod E, F and G (Figs. 5(b), (c) and (d), respectively). The black spots in Fig. 5(b) through (d) correspond to porosity and not to crystallized phases. The XRD spectrum for Rod E shown in Fig. 6(c) only displays broad peaks associated with amorphous structure consistent with the BSE image. On the contrary, the XRD spectra obtained for Rod F and G shown in Fig. 6 display diffraction peaks despite the lack of evidence of crystallization in the BSE images. In the XRD spectrum for Rod F shown in Fig. 6(b), peaks corresponding to t-ZrO_2, i-phase and one or more unknown phases are evident. Peaks corresponding to t-ZrO_2 and the unknown phases are evident in the XRD spectrum for Rod G shown in

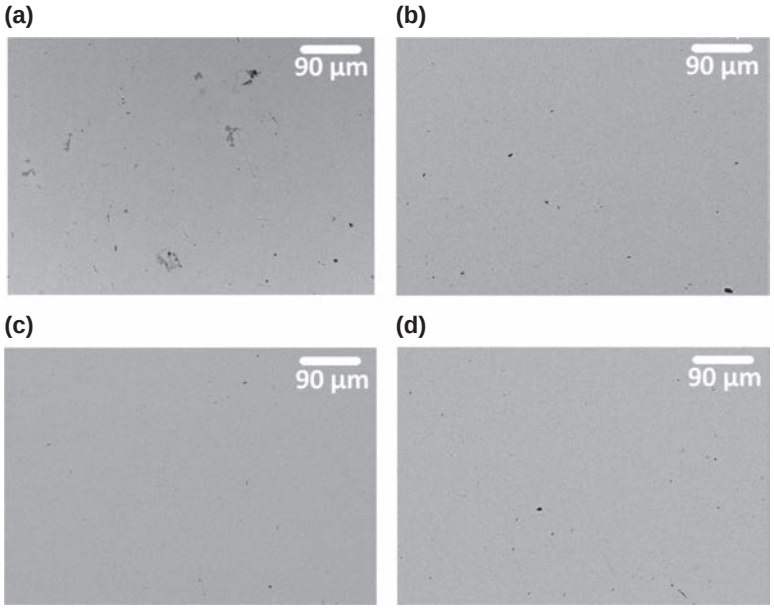

Fig. 5 BSE images of the middle sections of (a) Rod A, (b) Rod E, (c) Rod F and (d) Rod G.

Table 3 Argon and Zr purities used in the production of Rod A, E, F and G.

Rod	Ar purity	Zr purity
G	6.0	99.95%
F	4.8	99.95%
E	6.0	99.5%
A	4.8	99.5%

Table 4 Impurity content of Ar purge gas and raw Zr.

	[O] (ppm)	[Hf] (ppm)
6.0 Argon	< 1	—
4.8 Argon	< 8	—
99.95% Zr	580	29
99.5% Zr	1400	10,000

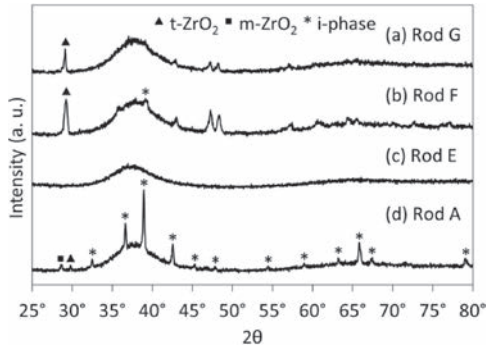

Fig. 6 XRD spectra for the middle sections of rods produced using different argon and raw Zr purities: (a) Rod G, (b) Rod F, (c) Rod E and (d) Rod A.

Fig. 6(a). The unknown phases were left unidentified since adequate matches in the International Centre for Diffraction Data (ICDD) Powder Diffraction Files (PDF) could not be found. The peak around 30° in both spectra most closely corresponds to tetragonal ZrO_2, although a small deviation from that of pure t-ZrO_2 is evident and maybe related to impurity substitution (e.g. Hf). Further transmission electron microscopy (TEM)/STEM work may be required to identify the unknown phases.

It was expected that increasing the purity of both Ar and Zr would increase GFA since crystallization of Zr-based BMGs had been widely reported to be promoted by oxygen.[12–14] However, Fig. 6 shows that the highest GFA was obtained in Rod E using low purity Zr (99.5%) and high purity Ar (Grade 6.0). This suggests that the relationship between oxygen concentration and GFA in Zr-based BMGs may not be monotonic as commonly described in literature. The effect of Hf concentration must also be considered since it varies the most between the different grades of Zr compared to the concentrations of the other impurities.

The increase in GFA between Rod A and E can be considered independent of Hf concentration since both rods were produced using the same grade of Zr. Comparing the XRD spectra in Fig. 6 for Rod A and E, it can be seen that increasing Ar purity suppresses i-phase and t-ZrO_2 formation. The suppression of i-phase formation with increasing Ar purity (i.e. decreasing oxygen content) is consistent with reports of i-phase stabilization by oxygen in literature.[13,17] The XRD spectra for Rod F and G in Fig. 6 are nearly identical suggesting that changes in oxygen concentration within this concentration range has little effect on GFA.

Unlike oxygen concentration, the effect of Hf concentration cannot be isolated based on the XRD spectra in Fig. 6 since with changing Zr purity, both the concentration of oxygen and Hf vary. Deduction of the effect of Hf can be attempted by comparing the XRD spectra for either Rod F or G in Fig. 6 with the XRD spectra for Rod A and E separately. Comparing the spectra for Rod F and G with that for Rod E, it can be hypothesized that the increase in the concentration of Hf resulted in an increase in GFA. However, the work of Liu *et al.* showed that micro-alloying of Hf in a Zr-Cu-Al-Ni alloy decreased GFA by promoting the formation of

$Cu(Zr,Hf)_2$.[18] By comparing the XRD spectra of Rod F and G with Rod A, it can be hypothesized that decreasing Zr purity resulted in the favourable formation of i-phase due to stabilization by Hf. Currently, there are no reports in literature of this phenomenon. Contrarily, i-phase stabilization by oxygen is widely reported. Further studies must be performed to determine whether Hf stabilizes i-phase. In the absence of results from this work, it will be assumed that the stabilization of the icosahedral phase is solely due to oxygen.

Still, the question remains: why is GFA optimized within a certain range of oxygen concentration? The peak around 30° corresponds to tetragonal ZrO_2 in the XRD spectra for Rod F and G in Fig. 6. The degradation of GFA at lower oxygen concentrations is most likely due to heterogeneous nucleation of intermetallics on the surface of the oxide particles. It may seem counter-intuitive that the rods produced with high purity Zr and Ar would contain an increased amount of oxide particles. However, this may be due to the destabilization of the icosahedral quasicrystalline phase with decreasing oxygen. As reported by Murty *et al.* in Zr-Cu-Al BMGs, the icosahedral units in the quasicrystalline phase include oxygen in its structure.[17] Based on this, the stabilization of the quasicrystalline phase could effectively suppress oxide formation. This is consistent with the trace amount of quasicrystalline peaks in the XRD spectra for Rod F and G in Fig. 6 compared to Rod A. It is currently unclear whether decreasing oxygen content stabilizes the unknown phases in addition to destabilizing the icosahedral phase. It can only be stated that below some oxygen concentration, the unknown phases are more stable than the icosahedral phase. This explanation may provide reasoning for the spectra for Rod A, G and F, but still does not provide reasoning for the high GFA of Rod E. To further investigate the two possibilities, the crystallization behaviour upon heating of each alloy was investigated using isochronal DSC. In the DSC plots for each alloy shown in Fig. 7 it can be seen that the rods with lower oxygen content (Rod G and F) contain one exothermic crystallization peak whereas the rods with higher oxygen content (Rod E and A) contain two. The second crystallization peak in the DSC plots for Rod A and E can be seen more clearly in Fig. 8. This is consistent with studies by Eckert *et al.*,[13] Gebert *et al.*,[19] and Murty *et al.*[17] who reported that increasing oxygen promotes a two-stage crystallization process in Zr-based bulk metallic glasses in which the formation of metastable phases is followed by transformation into equilibrium phases.

The glass transition temperatures (T_g), onset crystallization temperatures (T_x), supercooled liquid region (ΔT_x) and crystallization enthalpies (ΔH_c) extracted from the DSC plots can be seen in Table 5. It can be seen that ΔT_x decreases with increasing oxygen content suggesting that oxygen decreases the thermal stability of the glassy phase. This is consistent with findings reported by Eckert *et al.* in which a similar decrease in ΔT_x in Zr-Cu-Al-Ni BMGs was observed with increasing oxygen concentration.[13]

Interestingly, Rod E which has an intermediate oxygen concentration has the highest GFA. It should be noted that below the critical oxygen concentration for icosahedral quasicrystal formation (Rod F and G), the change in oxygen concentration seems to have little effect on the crystallization enthalpy. This suggests that the thermodynamics of crystallization and crystal fraction are unaffected. Above the critical oxygen concentration (Rod A and E), changes in oxygen concentration have a marked effect on crystallization enthalpy. The large decrease between the sums of the crystallization enthalpies in the DSC plots for Rod A and E, which reflects a difference in crystal fraction, suggests that GFA decreases rapidly when oxygen content is increased from the critical oxygen concentration necessary for icosahedral quasi-crystal formation.

XRD was used to determine the phases which formed after each exothermic peak in the DSC plot of Rod E to further examine its crystallization behaviour. In Fig. 9, it can be seen that an XRD spectra obtained for a specimen from Rod E heated past the first exothermic peak in the DSC scan closely matches the addition of XRD spectra for Rod A and G shown

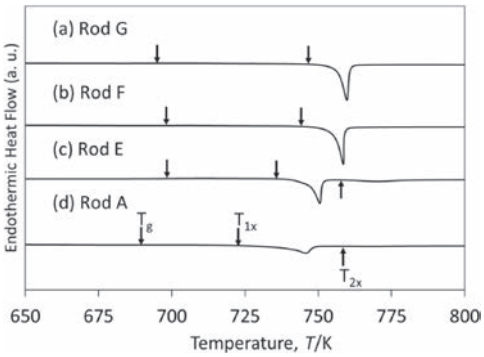

Fig. 7 DSC scans for samples produced with different argon purge gas and raw Zr purities: (a) Rod G, (b) Rod F, (c) Rod E and (d) Rod A.

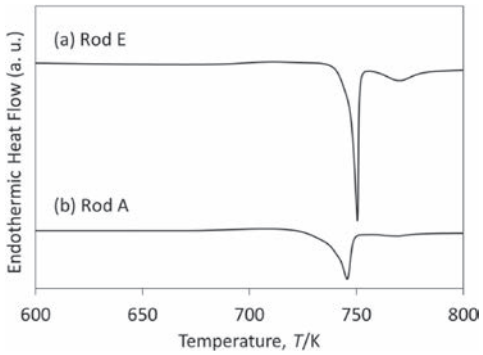

Fig. 8 DSC scans for samples produced with 99.5% Zr shown to emphasize the 2nd exothermic peak: (a) Rod E and (b) Rod A.

Table 5 Glass transition temperatures T_g, onset crystallization temperatures T_x, supercooled liquid regions ΔT_x and crystallization enthalpies ΔH_C for Rod A, E, F and G.

Rod	T_g (K)	T_x (K)		ΔT_x (K)	ΔH_C (kJ/mol)	
G	693	745		52	−4.06	
F	697	742		45	−4.07	
E	696	*Peak 1*	*Peak 2*	38	*Peak 1*	*Peak 2*
		734	756		−3.69 ± 0.08	−0.75 ± 0.01
A	688	*Peak 1*	*Peak 2*	33	*Peak 1*	*Peak 2*
		721	757		−2.36	−0.13

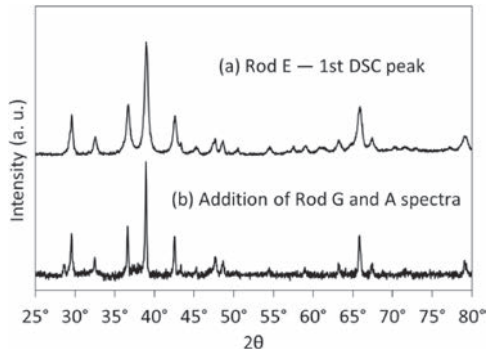

Fig. 9 XRD spectra for (a) Rod E heated past the 1st exothermic DSC peak and (b) the addition of the as-cast Rod G and A after removing the background and broad amorphous peaks.

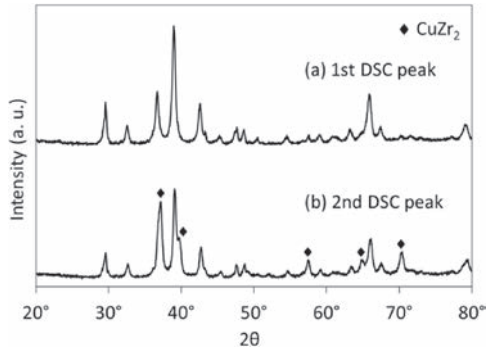

Fig. 10 XRD spectra for specimens from Rod E heated past the exothermic peaks in the DSC scan: (a) first peak and (b) second peak.

in Fig. 6 (after removing the background and broad amorphous peaks) which suggests that t-ZrO_2, the i-phase, unknown phases were all formed during this exothermic event.

In the XRD spectra for Rod E after being heated past the second exothermic DSC peak shown in Fig. 10, it can be clearly seen that the icosahedral phase transforms into the equilibrium $CuZr_2$ phase as the intensities of the peaks corresponding to the icosahedral phase decreased while those corresponding to $CuZr_2$ appeared. The intensities of the peaks corresponding to the unknown phases seem to be relatively unchanged after the second exothermic peak suggesting that it either does not transform into $CuZr_2$ or the kinetics involved in this transformation are sluggish. If the latter is true, increasing oxygen concentration may result in the kinetics of the formation of the unknown phases to become more sluggish. If so, there may be some critical oxygen content in which the GFA of this alloy is optimized due to both a low stability of the icosahedral quasi-crystalline phase and sluggish formation kinetics of the unknown phases. Contrarily, the high GFA at the critical oxygen content may be due to balancing of the driving forces of the icosahedral and unknown phases which consequently disrupts the formation of all phases by phase competition. This phenomenon is discussed by Shen *et al.*[20] and Deng *et al.*[21] In any case, the data shown here displays that there is a critical oxygen content at which GFA is optimized, and this has not been shown in any previous work. Further study will have to be performed to conclusively discern the origin of this phenomenon.

In summary, the high GFA of Rod E can still be attributed to the balancing of the stabilities of i-phase and t-ZrO_2. At low oxygen concentrations, t-ZrO_2 favourably precipitates during rapid cooling and leads to further GFA degradation by providing heterogeneous nucleation sites which promote the formation of the unknown phases. At high oxygen concentrations, GFA is degraded by the favourable formation of i-phase. Within a critical range of oxygen concentration, GFA is optimized by suppressing both t-ZrO_2 and i-phase formation.

4. Conclusion

In this study, we studied the effect of processing variables in arc melting and suction casting on the glass forming ability of Zr-based bulk metallic glasses. Homogeneity was effectively obtained using multiple melting iterations and increased melting durations. The cut and re-cast method was able to produce adequate homogeneity and slightly reduce oxidation, but at the expense of local inhomogeneity. It was found that the oxygen content can be controlled with greater ease by adjusting the purity of the Ar purge gas and raw Zr, rather than modifying the homogenization protocol.

The difference between input and actual Zr concentration was shown to be significant in arc melting and suction casting. This is possibly due to the formation of a Zr/ZrO_2-rich oxide layer during melting. As such, it should be noted that reported nominal compositions may be significantly different than actual compositions. When producing Zr-based BMG by arc melting and suction casting, the nominal composition may need to contain more Zr than the desired target composition.

The purity of the Ar purge gas and raw Zr were shown to markedly affect GFA. It is suggested that this is a result of varying oxygen concentrations. It was found that GFA is optimized when oxygen concentration is at a critical value. Simply increasing the purities of Ar and raw materials may not increase GFA.

Acknowledgments

This work was funded by the Natural Sciences and Engineering Research Council of Canada (NSERC) and Gedex Inc. through the Collaborative Research Grant program. Funding was also provided by the Department of Materials Science and Engineering of the University of Toronto through the Haultain Fellowship award. The authors gratefully acknowledge their support.

REFERENCES

1) A. L. Greer: Science **267** (1995) 1947–1953.
2) A. Inoue: Acta Mater. **48** (2000) 279.
3) W. H. Wang, C. Dong and C. H. Shek: Mater. Sci. Eng. R **44** (2004) 45–89.
4) A. Inoue and T. Zhang: Mater. Trans. **37** (1996) 185–187.
5) N. Nishiyama, K. Takenaka, H. Miura, N. Saidoh, Y. Zeng and A. Inoue: Intermetallics **30** (2012) 19–24.
6) K. J. Laws, B. Gun and M. Ferry: Metall. Mater. Trans. A **40** (2009) 2377–2387.
7) Q. K. Jiang, G. Q. Zhang, L. Yang, X. D. Wang, K. Saksl, H. Franz, R. Wunderlich, H. Fecht and J. Z. Jiang: Acta Mater. **55** (2007) 4409–

4418.
8) N. Khademian, R. Gholamipour, F. Shahri and M. Tamizifar: J. Alloy. Compd. **546** (2013) 41–47.
9) P. Li, G. Wang, D. Ding and J. Shen: J. Non-Cryst. Solid **358** (2012) 3201.
10) W. ZengRui, D. DanDan, Q. JianBing, W. Qing, W. YingMin and D. Chuang: Sci. China Phys. Mech. Astron. **56** (2013) 1419–1422.
11) Q. Zhang, W. Zhang and A. Inoue: Mater. Trans. **47** (2006) 2804.
12) Z. Altounian, E. Batalla, J. O. StromOlsen and J. L. Walter: J. Appl. Phys. **61** (1987) 149–155.
13) J. Eckert, N. Mattern, M. Zinkevitch and M. Seidel: Mater. Trans. **39** (1998) 623–632.
14) X. H. Lin, W. L. Johnson and W. K. Rhim: Mater. Trans. **38** (1997) 473–477.
15) L. Liu and K. C. Chan: Appl. Phys. A **80** (2005) 1739–1742.
16) P. A. Bancel, P. A. Heiney, A. I. Goldman and P. M. Horn: Phys. Rev. Lett. **54** (1985) 2422–2425.
17) B. S. Murty, D. H. Ping, K. Hono and A. Inoue: Acta Mater. **48** (2000) 3985–3996.
18) L. Liu, C. L. Qiu, H. Zou and K. C. Chan: J. Alloy. Compd. **399** (2005) 144–148.
19) A. Gerbert, J. Eckert and L. Schulz: Acta Mater. **46** (1998) 5475–5482.
20) J. Shen, J. Zou, L. Ye, Z. P. Lu, D. W. Xing, M. Yan and J. F. Sun: J. Non-Cryst. Solids **351** (2005) 2519–2523.
21) S. T. Deng, H. F. Zhang, A. M. Wang, H. Li, B. Z. Ding and Z. Q. Hu: J. Alloy. Compd. **460** (2008) 182–185.